Temperature Dependence of the Rotation and Hydrolysis Activities of F_1-ATPase

Shou Furuike,* Kengo Adachi,* Naoyoshi Sakaki,† Rieko Shimo-Kon,* Hiroyasu Itoh,‡§ Eiro Muneyuki,¶ Masasuke Yoshida,‖** and Kazuhiko Kinosita Jr.*

Department of Physics, Faculty of Science and Engineering, Waseda University, Shinjuku-ku, Tokyo, Japan; †Institute of Industrial Science, University of Tokyo, Meguro-ku, Tokyo, Japan; ‡Tsukuba Research Laboratory, Hamamatsu Photonics KK, and §CREST "Formation of Soft Nano-Machines" Team 13, Tokodai, Tsukuba, Japan; ¶Department of Physics, Faculty of Science and Engineering, Chuo University, Tokyo, Japan; ‖Chemical Resources Laboratory, Tokyo Institute of Technology, Nagatsuta, Yokohama, Japan; and **ICORP ATP Synthesis Regulation Project, Japan Science and Technology Agency (JST), Aomi, Tokyo, Japan

ABSTRACT F_1-ATPase, a water-soluble portion of the enzyme ATP synthase, is a rotary molecular motor driven by ATP hydrolysis. To learn how the kinetics of rotation are regulated, we have investigated the rotational characteristics of a thermophilic F_1-ATPase over the temperature range 4–50°C by attaching a polystyrene bead (or bead duplex) to the rotor subunit and observing its rotation under a microscope. The apparent rate of ATP binding estimated at low ATP concentrations increased from 1.2×10^6 M^{-1} s^{-1} at 4°C to 4.3×10^7 M^{-1} s^{-1} at 40°C, whereas the torque estimated at 2 mM ATP remained around 40 pN·nm over 4–50°C. The rotation was stepwise at 4°C, even at the saturating ATP concentration of 2 mM, indicating the presence of a hitherto unresolved rate-limiting reaction that occurs at ATP-waiting angles. We also measured the ATP hydrolysis activity in bulk solution at 4–65°C. F_1-ATPase tends to be inactivated by binding ADP tightly. Both the inactivation and reactivation rates were found to rise sharply with temperature, and above 30°C, equilibrium between the active and inactive forms was reached within 2 s, the majority being inactive. Rapid inactivation at high temperatures is consistent with the physiological role of this enzyme, ATP synthesis, in the thermophile.

INTRODUCTION

F_1-ATPase is an ATP-driven rotary molecular motor in which the central γ-subunit rotates against a surrounding cylinder made of $\alpha_3\beta_3$ subunits arranged alternately (1–5). ATP hydrolysis occurs in three catalytic sites, each hosted primarily by a β-subunit (1). As expected, rotation proceeds basically in steps of 120°, each coupled to consumption of one ATP molecule (6,7). Direction of rotation is counterclockwise when viewed from the side of γ-protrusion (3), and the three β-subunits have been shown to bind ATP sequentially in this direction (8). The F_1 is a reversible molecular machine in that reverse rotation of γ by an external force results in ATP synthesis (9,10). The reversal of chemical reaction (ATP hydrolysis) by manipulation of the γ-angle alone implies a γ-dictator mechanism, in which the orientation of the γ-rotor relative to the $\alpha_3\beta_3$ stator determines which of the chemical reactions (binding/release of ADP, phosphate, and ATP, and synthesis/hydrolysis of ATP) is to occur in each catalytic site (5). The basic coupling scheme for hydrolysis-driven rotation has been worked out for an F_1-ATPase of thermophilic origin (11). The 120° rotational step is split into 80–90° and 40–30° substeps (12), which we refer to here as 80° and 40° substeps. The first 80° substep is initiated and driven by ATP binding (12). ADP release occurs immediately after ATP binding (at least when rotation is slowed down by an external force), and the release assists the 80° substep (11). An ATP is hydrolyzed in the interim between 80° and 40° substeps (13), after the ATP has been bound at 0° and 200° rotation has taken place (8). Another event at the 80° interim is phosphate release, which initiates and drives the last 40° rotation (11). The ATP hydrolysis and phosphate release at 80° both take ~1 ms (11,12), whereas ATP binding at 0° is fast with a bimolecular rate of $\sim 2 \times 10^7$ M^{-1} s^{-1} (12). Above the apparent Michaelis-Menten constant, K_m, of ~15 μM, therefore, the rate-limiting processes are the two reactions at 80°.

The scheme above was obtained at room temperature (23°C), whereas the optimum temperature for the thermophilic enzyme is ~75°C (14). A different scheme(s) may apply at different temperatures, and the temperature dependence of the rate-limiting process(es) may reveal the nature of that process. Here, we have investigated the temperature dependence of rotation and hydrolysis of the F_1-ATPase derived from a thermophile *Bacillus* PS3. We used its minimal subcomplex $\alpha_3\beta_3\gamma$, which is active in rotation and hydrolysis, and refer to it simply as F_1. Unexpected findings are that a new rate-limiting step emerges at low temperatures and that F_1 quickly falls into an inhibited state at high temperatures.

Submitted October 18, 2007, and accepted for publication March 10, 2008.

Address reprint requests to Kazuhiko Kinosita Jr., Dept. of Physics, Faculty of Science and Engineering, Waseda University, 3-4-1 Okubo, Shinjuku-ku, Tokyo 169-8555, Japan. Tel.: 81-3-5952-5871; Fax: 81-3-5952-5877; E-mail: kazuhiko@waseda.jp.

Editor: David D Hackney.

0006-3495/08/07/761/10 $2.00

doi: 10.1529/biophysj.107.123307

MATERIALS AND METHODS

Reagents

Nucleotides (ATP and ADP) were purchased from Roche Diagnostics (Basel, Switzerland), bovine serum albumin (BSA, ultrapure) from Nacalai Tesque (Kyoto, Japan), and glass coverslips from Matsunami (Osaka, Japan).

Purification of F_1

A mutant (α-C193S, β-His_{10} at amino terminus, γ-S107C, and γ-I210C) $\alpha_3\beta_3\gamma$ subcomplex derived from thermophilic *Bacillus* PS3 was expressed in *Escherichia coli* and purified as described (15). Briefly, cell lysate was heat-treated (15 min at 65°C), and denatured *E. coli* proteins were removed by centrifugation. The supernatant was sequentially passed through a Ni^{2+}-nitrilotriacetic acid (Ni-NTA) superflow column (Qiagen, Hilden, Germany) and a butyl-Toyopearl column (Tosoh, Tokyo), and we collected the fractions most abundant in F_1 as judged by SDS- and native-polyacrylamide gel electrophoresis. For storage and condensation, F_1 was precipitated in 70% ammonium sulfate containing 1 mM dithiothreitol (DTT) and kept at 4°C.

Rate of ATP hydrolysis

Precipitated F_1 was dissolved in a buffer (100 mM potassium phosphate, pH 7.0, 2 mM EDTA, and 1 mM DTT) and passed through a size exclusion column (Superdex 200 HR 10/30; Amersham Biosciences, Piscataway, NJ), preequilibrated with 100 mM potassium phosphate, pH 7.0, and 2 mM EDTA, to remove DTT and possible denatured enzymes. The concentration of F_1 was determined from the absorbance at 280 nm by assuming an extinction coefficient of 154,000 M^{-1} cm^{-1} (15,16). Tightly bound nucleotides (ATP or ADP) that remained on F_1 were <0.05 mol/mol F_1, as confirmed with reverse-phase high-performance liquid chromatography (TSK-GEL ODS-80Ts, Tosoh) (17).

The rate of ATP hydrolysis was measured, before biotinylation, with an ATP regeneration system that consisted of 0.2 mM NADH (nicotinamide adenine dinucleotide), 2.5 mM phosphoenolpyruvate, 0.5 mg ml^{-1} pyruvate kinase (rabbit muscle, Roche) and 0.1 mg ml^{-1} lactate dehydrogenase (hog muscle, Roche) in buffer A (10 mM MOPS (3-(*N*-morpholino)propanesulfonic acid)-KOH, pH 7.0, 50 mM KCl, and 2 mM $MgCl_2$). For measurements at 50–65°C, we used heat-stable enzymes of *Bacillus stearothermophilus*: pyruvate kinase (100 units ml^{-1} at 30°C; Unitika, Osaka, Japan) and lactate dehydrogenase (50 units ml^{-1} at 30°C; Sigma, St. Louis, MO). At 50°C, these two enzyme systems gave similar results for the hydrolysis activity of F_1 (the hydrolysis activity above 50°C assessed with the heat-stable enzymes is underestimated because these enzymes did not operate fast enough).

The hydrolysis reaction was monitored as the disappearance of NADH absorbance at 340 nm (16,18) in a thermostatted spectrophotometer (U-3300, Hitachi, Tokyo) equipped with a magnetic stirrer. The sample cuvette containing a stirrer tip was sealed with a Teflon cap to prevent evaporation, and the sample chamber was purged with nitrogen to avoid frosting. Before each measurement, we preincubated the ATP regenerating system above (1950 μl) in the spectrophotometer while monitoring the temperature with a thin thermocouple immersed in the cuvette. When the temperature reached a desired value, we added a desired amount of MgATP (40 μl), which had separately been preincubated at the same temperature. Finally, we placed 10 μl of 1 μM F_1, kept at room temperature, on a plastic cuvette mixer which had been preincubated at the final temperature, and rapidly mixed it in the cuvette. Mixing took up to 2 s, and thus we report hydrolysis kinetics after 2 s. We calculated the hydrolysis activity at 2-s intervals by first averaging absorbance values in 2-s bins and then dividing differences between every other bin by (6220 M^{-1} cm^{-1} ($\varepsilon_{340nm}^{NADH}$) $\times$ 1 cm (optical path) $\times$ 5 nM (F_1 concentration) $\times$ 4 s (time difference)). At high temperatures, the absorbance slightly decreased with time before the addition of F_1; this baseline drift was corrected for.

Rotation assay

The sole two cysteines (γ-S107C and γ-I210C) on the protruding portion of γ were biotinylated by incubation with a twofold molar excess of 6-(*N*′-(2-(*N*-maleimido)ethyl)-*N*-piperazinylamido)hexyl-D-biotinamide (Dojindo, Kumamoto, Japan) for 1 h at room temperature, and unbound biotins were removed on a Superdex 200 HR 10/30 column (18). Biotinylated F_1 was frozen with liquid nitrogen and stored at −80°C.

Biotinylated F_1 (500 pM) in buffer A was infused into an observation chamber which was constructed of two coverslips: a bottom one (24 $\times$ 32 mm^2) modified with Ni-NTA (9) and an untreated top one (18 $\times$ 18 mm^2). After waiting for a few minutes to let F_1 bind to the Ni-NTA surface, we washed the chamber with five volumes of buffer A, and infused 0.5–5 mg ml^{-1} BSA in buffer A to prevent nonspecific adsorption of beads. After incubation for 5–10 min, we infused ~0.1% (w/v) streptavidin-coated beads (nominal diameter 0.29 or 0.49 μm, Seradyn, Indianapolis, IN, or Bangs, Fishers, IN) in buffer A containing 0.5–5 mg ml^{-1} BSA. After 30 min, unbound beads were washed out with more than five chamber volumes of buffer A. Finally we infused buffer A containing a desired amount of ATP (2 mM Mg^{2+} in excess over ATP) and an ATP-regenerating system consisting of 0.02–0.2 mg ml^{-1} creatine kinase (rabbit muscle, Roche) and 2.5 mM creatine phosphate (Roche). Above 40°C, the ATP-regenerating system was omitted because creatine kinase would be denatured. The observation chamber was sealed with silicone grease to avoid evaporation.

Bead rotation was observed on an inverted microscope (IX70, Olympus, Tokyo, Japan) using a super long working distance objective lens (SLCPlanFl, 40×, NA 0.55, Olympus). To measure rotation over a wide range of temperatures, we used a stable microscope stage (KS-O, ChuukoushaSeisakujo, Tokyo, Japan) that substantially reduces thermal drift. On the stage, we placed a custom temperature-controlled specimen holder (MATS-1000FST, Tokai Hit, Shizuoka, Japan), as shown in Fig. 1. Images were captured with a high-speed CMOS camera (FASTCAM-F1-DJV, Photron, Tokyo, Japan) at 500 frames s^{-1}. Centroids of bead images were calculated as described (12).

In some experiments at 4°C, we used gold beads with a nominal diameter of 100 or 150 nm (BBInternational, Cardiff, UK) to observe rotation under a

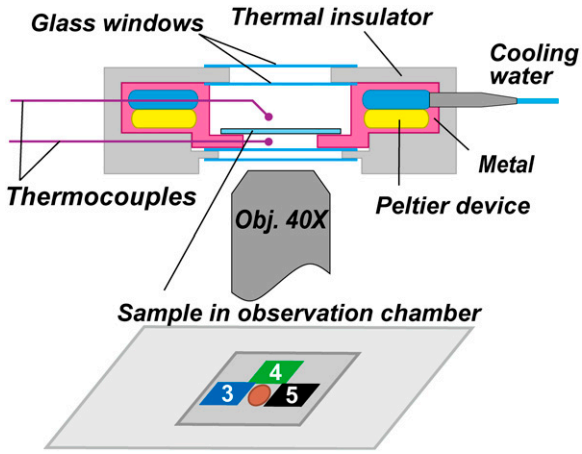

FIGURE 1 Sectional view of the temperature-controlled specimen holder. Inner walls and the bottom are constructed of steel plates, which contact with Peltier devices of temperature range 0–70°C. Temperatures immediately above and below the sample (coverslip observation chamber) are monitored by two thermocouples. Small pieces of thermochromic liquid-crystal film are attached to the top surface of the chamber to read the sample temperature to within ±1°C. The example shown is for the measurement at 4°C, where pieces 3–5, respectively, respond to 3–5°C, and the sample area shown in brown is observed. In some measurements, an identical set of thermochromic film was also attached to the bottom surface; the readings of the top and bottom agreed within 1°C.

low viscous load. To attach a gold bead to the biotinylated F_1, we functionalized the gold beads with Neutravidin (Pierce, Rockford, IL). To 1 ml of 100-nm gold beads (EM.GC100, 5.6×10^9 particles ml^{-1}) or 150-nm beads (EM.GC150, 1.7×10^9 particles ml^{-1}), we added 5 μl of 5 mg ml^{-1} Neutravidin, 0.5 mM dithiobis[succinimidylpropionate] (Pierce), and 10 mM tris(2-carboxyethyl)phosphine (Pierce) in buffer B (buffer A without $MgCl_2$). In the case of 150-nm beads, we also added 10 μl of 2 mM 2-aminoethanethiol (Tokyo Chemical Industry, Tokyo, Japan) and 40 mM NHS-m-dPEG (molecular weight 1214, Quanta BioDesign, Powell, OH) in buffer B. The reaction was allowed to proceed at room temperature for 2 h. Then the suspension was kept at 4°C for up to 2 weeks. Before use, the beads were washed ≥4 times with 10 mM HEPES (2-[4-(2-hydroxyethyl)-1-piperazinyl]ethanesulfonic acid), pH adjusted to 8.0 with KOH. To observe the small gold beads, we sandwiched the observation chamber between a 50× NA 0.5 lens and a 100× NA 1.4 objective lens from above and below via immersion oil. The temperature of both objectives was controlled with circulating water, and the sample temperature was confirmed with a thin thermocouple (diameter 50 μm, Ishikawa Trading, Tokyo, Japan) placed inside the observation chamber. Images were captured at 2000 frames s^{-1}.

We estimated the torque that F_1 produces assuming that the rotary speed is limited by viscous friction against the rotating bead (5): when a spherical bead of radius a rotates at speed ω (in radians s^{-1}), the torque N is given by

$$N = \omega\xi, \tag{1}$$

$$\xi = 8\pi\eta a^3 + 6\pi\eta a x^2, \tag{2}$$

where ξ is the frictional drag coefficient, x is the rotation radius, i.e., the distance between the bead center and rotation axis, and η is the viscosity of the medium. We took η as that of water at respective temperatures (19). The viscosity of buffer A, measured with a viscometer (Ubbelohde (SU) No. 0B, Shibata, Tokyo, Japan) at 25°C and 3°C, agreed with the water values to within 5%, whether 0.2 mg ml^{-1} creatine kinase was included or not. Equation 2 does not take into account the higher effective viscosity near a glass surface (20), and thus leads to an underestimate of the torque.

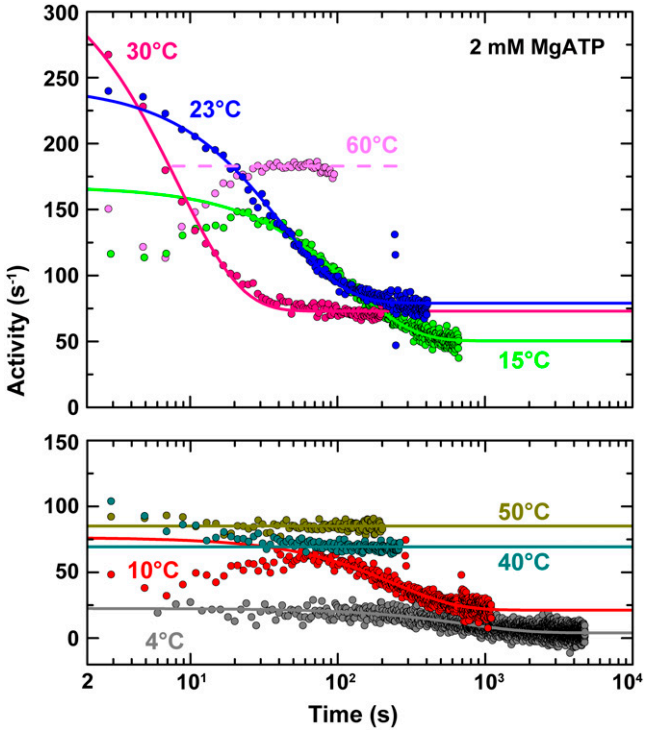

FIGURE 2 Typical time courses of hydrolysis activity at different temperatures (shown in two panels for clarity). The reaction was started at time 0 by adding F_1 to buffer A containing 2 mM MgATP and an ATP regeneration system consisting of 0.2 mM NADH, 2.5 mM phosphoenolpyruvate, 0.5 mg ml^{-1} pyruvate kinase (0–50°C, from rabbit muscle; 50–65°C, from thermophilic bacterium), and 0.1 mg ml^{-1} lactate dehydrogenase (0–50°C, from hog muscle; 50–65°C, from thermophilic bacterium). Smooth curves are fit with Eq. 3 to the portion excluding the initial lag period. The apparent lag at 60°C is due to a low activity of the thermophilic regeneration system; also, the performance of this regeneration system was gradually degraded with time at high temperatures, limiting the measurement to a relatively short period.

RESULTS

Temperature dependence of the hydrolysis activity

In the previous study (14), the ATP hydrolysis activity of the thermophilic F_1 has been shown to be maximal at 75°C, with another peak at 20°C. The activity was assessed as the amount of phosphate released over a 10-min period, and thus the values correspond to the activity at steady-state, where active and inactive (MgADP-inhibited) forms of the enzyme coexist and interchange with each other (16,21,22). Here we have coupled the ATP hydrolysis with the consumption of NADH and monitored the time course of hydrolysis from 2 s after mixing nucleotide-free F_1, which is supposed to be uninhibited.

The hydrolysis activity at 2 mM MgATP was time-dependent, except at 35–50°C where the activity was apparently constant from the beginning (Fig. 2). Above 50°C, we observed an apparent lag (up to ~30 s at 60°C in Fig. 2), but this is due to low activity of the heat-stable ATP regeneration system used at these temperatures, as confirmed by adding ATP to the system. Presumably, the hydrolysis activity of F_1 above 50°C is also time-independent, as at 35–50°C. At intermediate temperatures of 23–30°C, the hydrolysis activity was maximal at the start of the measurement (2 s) and decreased to a constant steady-state value. Here, (almost) all F_1 molecules in solution probably engaged in hydrolysis at the beginning, whereas MgADP inhibition set in as time passed. At lower temperatures, the maximal activity was preceded by a lag period with lower activity that could not be explained by the regenerating system, which worked sufficiently fast. (The data for 4°C in Fig. 2 also showed a slow increase in activity up to ~200 s, except for the first several points, which happened to be relatively high in this particular record). The cause for the low-temperature lag is unknown; a possibility is that the binding of a second ATP to the nucleotide-free F_1, required to fill two of the three catalytic sites of F_1 to let it engage on the normal reaction pathway (11), is extremely slow at low temperatures. Alternatively, binding of ATP to noncatalytic nucleotide binding sites (hosted primarily by an α-subunit) may be required for fully active catalysis (18), and this binding may be slow at low temperatures. In accordance with, but not as proof of, the latter possibility, a mutant F_1 lacking noncatalytic sites did not show a lag in activity at 15°C (data not shown). Whatever the cause may be, the lag is shorter than

the time over which the MgADP inhibition develops, and thus we neglect the lag in the analysis below.

Except for the relatively short lag at low temperatures, the time courses of the activity change, $A(t)$, at 4–50°C could be approximated by

$$A(t) = (A_{\text{init}} - A_{\text{ss}})\exp(-k_{\text{app}}t) + A_{\text{ss}}, \quad (3)$$

where A_{init} and A_{ss} are the initial and steady-state activities, and k_{app} the apparent rate constant (Fig. 2). At 35°C and above, the first exponential part was missing, but the temperature dependence of the three parameters (Fig. 3) suggests that the apparent absence is due to rapid relaxation compared to the mixing time of 2 s, and that A_{init} at these temperatures are actually much higher than the observed A_{ss}. The values of the steady-state activity A_{ss} here are somewhat higher but agree, within a factor of ~2, with the previous estimate (14).

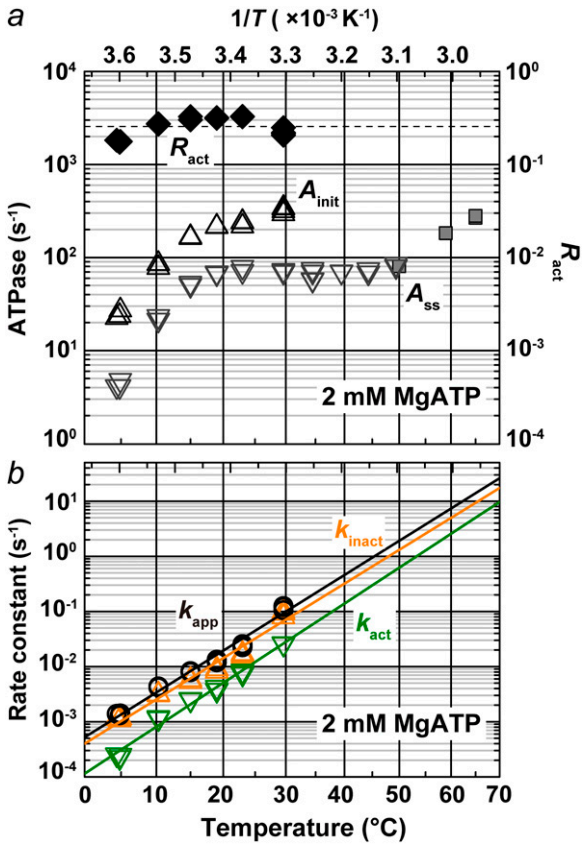

FIGURE 3 Temperature dependence of the parameters characterizing the hydrolysis activity at 2 mM MgATP. (*a*) The initial (A_{init}) and steady-state (A_{ss}) activities are indicated by triangles and inverted triangles, respectively. The steady-state values obtained with the thermophilic regeneration system (*gray squares*) are likely underestimated. The fraction of active F_1 at steady state ($R_{\text{act}} = A_{\text{ss}}/A_{\text{init}}$) is indicated by black diamonds. (*Dashed line*) Average of R_{act} between 4 and 30°C; T, absolute temperature. (*b*) The black line represents the apparent rate constant, k_{app}, for the relaxation from the initial high-activity state to the steady state, and indicates an activation energy of 120 kJ K^{-1} mol^{-1}. Green and orange lines indicate the rate constants for the conversion from active to inactive (k_{inact}) and from inactive to active (k_{act}) states, respectively, with activation energies of 119 kJ K^{-1} mol^{-1} and 126 kJ K^{-1} mol^{-1} for k_{inact} and k_{act}, respectively.

The interpretation of Eq. 3 is that A_{init} represents the activity of active F_1 and A_{ss} the average activity of the equilibrium mixture of active and inactive, or inhibited, F_1:

$$[\text{active } F_1] \underset{k_{\text{act}}}{\overset{k_{\text{inact}}}{\rightleftarrows}} [\text{inactive } F_1]; \quad (4)$$

$$R_{\text{act}} \equiv A_{\text{ss}}/A_{\text{init}} = [\text{active } F_1]_{\text{eq}}/\{[\text{active } F_1]_{\text{eq}} + [\text{inactive } F_1]_{\text{eq}}\} = k_{\text{act}}/(k_{\text{act}} + k_{\text{inact}}); \quad (5)$$

$$k_{\text{app}} = k_{\text{act}} + k_{\text{inact}}, \quad (6)$$

where R_{act} is the fraction of active F_1 at equilibrium. From Eqs. 5 and 6 and the experimental R_{act} and k_{app}, we obtain k_{act} and k_{inact}, which we plot in Fig. 3 *b*. The values at 23°C, $k_{\text{act}} = 0.007\ s^{-1}$ and $k_{\text{inact}} = 0.016\ s^{-1}$, are roughly consistent with those estimated in a previous study at 2 mM ATP and at 25°C of 0.018 s^{-1} and 0.034 s^{-1} (22).

Both k_{act} and k_{inact} rise sharply with temperature, whereas R_{act} remains nearly constant above 10°C or slightly decreases with temperature. If we assume that R_{act} behaves similarly above 35°C (Fig. 3 *a*, *dashed line*), A_{init} at 65°C, calculated from the observed (but likely underestimated) A_{ss} would be 1100 s^{-1}, corresponding to the rotary rate of 370 revolutions s^{-1}. In a preliminary experiment with 40-nm gold particles, we have been able to find a few particles to rotate at >700 revolutions s^{-1} at 50°C, suggesting that the rotary speed of this motor near the optimum temperature of ~70°C is indeed >1000 revolutions s^{-1}.

The steep decrease of A_{init} below ~10°C suggests that a different rate-limiting step begins to dominate at low temperatures, as confirmed below.

F_1 rotation at different temperatures

To visualize the rotation of the γ-subunit over a wide range of temperatures, we attach to the γ-subunit a polystyrene bead or its duplex, rather than an actin filament (3), which may be denatured or depolymerized at extreme temperatures (23). The temperature of the specimen holder in Fig. 1 could be controlled between 0°C and 70°C. At equilibrium, a static temperature gradient developed inside the holder: for example, when the temperature was set at 4°C, thermocouples placed above and below the coverslips reported 7.5°C and 3.0°C, respectively. We thus attached tiny pieces of thermochromic liquid-crystal film (T.L.C. 16 level, Thermographic Measurements, Flintshire, United Kingdom; each responds to a particular temperature with a precision of 1°C) directly on the bottom and top coverslips. Readings of the top and bottom surfaces were the same to within 1°C, which we took as the specimen temperature. Rotation was observed in a space (Fig. 1, *brown spot*) surrounded by two or more pieces of the thermosensor film. Thermal stabilization of the specimen holder took ~30 min, and we placed a coverslip observation chamber in the holder and waited for an additional ~10 min before starting to record rotation.

In preliminary experiments, we continuously watched the same F_1 molecules rotate while changing the temperature from 23°C to 4°C or 40°C. During cooling runs, which took ~30 min, we observed most rotating beads to decelerate, as implied in the behavior of A_{init} in Fig. 3 *a*. Some beads abruptly fell in a long pause, and recovery into the rotating state was noticeably longer at 4°C (usually >5 min, and thus we gave up) than at 23°C (often within a few minutes). In heating runs, in contrast, we often observed beads that did not rotate at 23°C begin rotating as the temperature increased. Rotating beads also fell in a pause and resumed rotating, and the alternating period was noticeably shorter at 40°C than at or below 23°C. Although we did not attempt quantitative analysis, these pausing characteristics are consistent with the temperature dependence of k_{act} and k_{inact} estimated from ATPase activity (Fig. 3 *b*).

We recorded rotation time courses at temperatures between 4°C and 40°C. Above 40°C, beads tended to detach from the glass surface during thermal equilibration (~10 min), and thus we could not record rotation for a long time. Typical records for 0.29-μm beads that rotated relatively fast and smoothly for >100 revolutions are shown in Fig. 4 (we could not ascertain whether these beads were single or duplex, because the resolution of the objective lens used was low). At the camera speed of 500 frames s^{-1} (2 ms/frame), clear dwells were not resolved at 40°C, and the time-averaged rotary speed at 40°C did not change appreciably between the saturating ATP concentration of 2 mM and a subsaturation level of 2 μM, indicating that the hydrodynamic friction against the bead(s) limited the rotary rate in these ATP concentrations and that chemical reactions including ATP binding were faster. Extrapolation of the rate of hydrolysis by active F_1 (Fig. 3 *a*, A_{init}) to 40°C would predict a value much higher than three times the rotary rate at 2 mM ATP, corroborating this interpretation. At 23°C, we observed clear 120° stepping at 2 μM ATP, which we ascribe to slow ATP binding (see below; also (12)). When we accumulated the angle histogram at 2 mM or 20 μM ATP over a period much longer than that in Fig. 4, we often found broad peaks at 120° intervals (not shown). This is likely due to the tendency of a large bead to stumble at positions ~80° past the ATP-waiting angles, where a reaction sensitive to mechanical hindrance takes place (18). At 4°C, all rotations were stepwise, irrespective of the ATP concentration. The dwells became longer at lower ATP concentrations, indicating that the dwells occur at ATP-waiting angles. At the camera speed of 500 frames s^{-1}, we did not observe clear dwells other than those separated by 120° in all ATP concentrations, and thus the dwells at the saturating ATP concentration of 2 mM must also be at or close to ATP-waiting angles.

These dwells observed at 4°C at the saturating ATP concentration may in part be due to hydrodynamic friction or surface obstruction that could impede the bead motion, because larger (0.49 μm) beads tended to prolong the dwells. To see whether these dwells are basically a genuine property of F_1 and whether these indeed occur at ATP-waiting angles, we observed rotation at 4°C with smaller, 100-nm or 150-nm, gold beads. The time-averaged rotation speeds of these beads were similar to each other and only about twice as high as the speed of the 0.29-μm plastic beads (Fig. 5 *a*), indicating that these gold beads do not impede rotation (frictional drag would be proportional to the cube of the bead size). Both 150-nm and 100-nm gold beads showed clear dwells separated by 120° (Fig. 5 *b*), implying that the dwells at 2 mM ATP at 4°C are genuine. The 100-nm beads also showed frequent and distinct dwells for several milliseconds at angles ~40° before the major dwell angles (Fig. 5 *b*), reminiscent of the 80° dwells observed at room temperature where F_1 waits for ATP hydrolysis and phosphate release (11). This observation strengthens our contention, above, that the long dwells at 2 mM ATP at 4°C are at or close to ATP-waiting angles.

In Fig. 6 we summarize the ATP dependence of rotary and hydrolysis rates. The hydrolysis rate is divided by 3 for direct comparison. The hydrolysis rate, which should correspond to the rate of unloaded rotation, clearly indicates that 2 mM ATP is saturating even at 4°C. At sufficiently low ATP concentrations, all rates were proportional to the ATP concentration. The slopes in the linear portion, either (hydrolysis rate (without division by 3))/[ATP concentration] or (3 × rotary rate)/[ATP concentration], give the apparent bimolecular rate of ATP binding, k_{on}^{app}, which we plot against temperature in Fig. 6 *b*; k_{on}^{app} for ATP hydrolysis could not be estimated above 30°C, where the initial burst was missing. At 23°C, k_{on}^{app} for rotation was 1.8×10^7 M^{-1} s^{-1}, in agreement with previous estimates of 2.6×10^7 M^{-1} s^{-1} using a 40-nm gold particle, for which hydrodynamic friction is negligible (12), and 1.5×10^7 M^{-1} s^{-1} using an actin filament (6). In principle, k_{on}^{app} estimated from rotation and hydrolysis should agree with each other. In fact, we have always observed the rotation rate to be slightly higher at 23°C, as is also the case in this study (Fig. 6 *b*), suggesting that some of the F_1 molecules in the hydrolysis assay are already inhibited or inactive in the early period where the ''initial'' rate is estimated. The rather large discrepancy at 4° here likely resulted from the initial lag observed in the hydrolysis time course (Fig. 2). The temperature dependence of k_{on}^{app} (Fig. 6 *b*) is similar to that of A_{init} (Fig. 3 *a*), the initial rate of hydrolysis, although we see no reason why ATP binding and the rate-limiting reaction(s) in the overall catalysis (which are ATP hydrolysis and phosphate release at 23°C) should show the same temperature dependence.

The saturation of rotary rate above 20 μM MgATP, except at 4°C, is due to the hydrodynamic friction against the rotating bead, as discussed above for the data at 40°C, and thus the saturation level is lower than that for hydrolysis, which was measured under unloaded conditions. The saturation of hydrolysis rate is due, at least at 23°C, to the two rate-limiting reactions at the 80° interim, ATP hydrolysis and phosphate release (11). At 4°C, the saturation levels for hydrolysis and

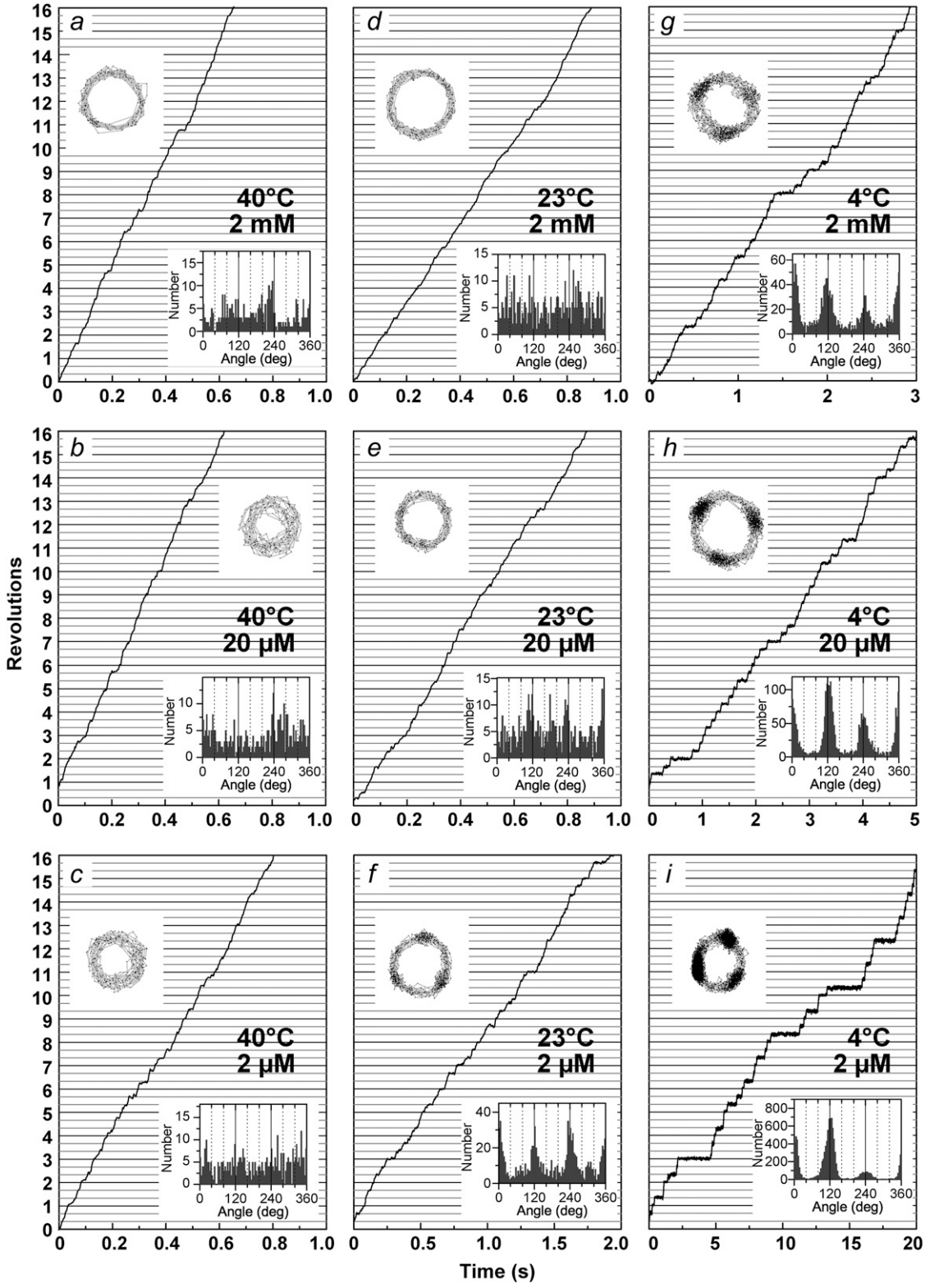

FIGURE 4 Time courses of rotation of 0.29-μm beads at indicated temperatures and ATP concentrations. (*Upper insets*) Trajectories of the bead centroids. (*Lower insets*) Histograms of angular positions for the indicated portion of the records.

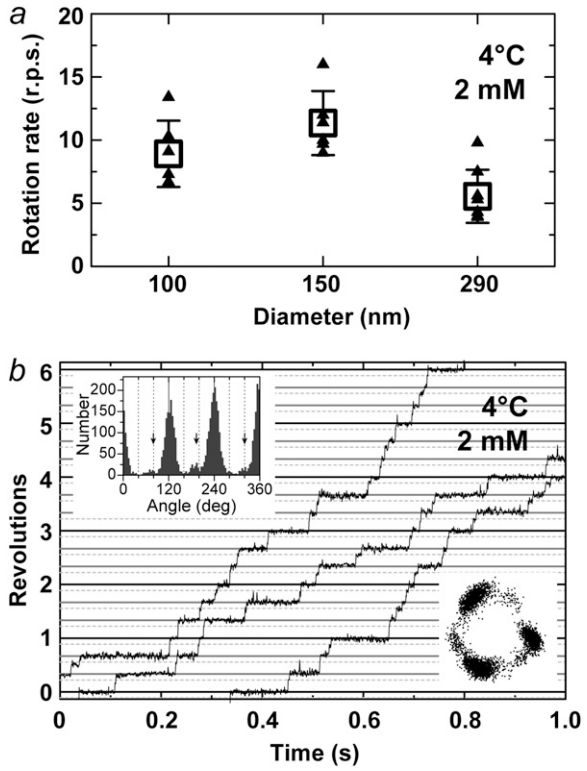

FIGURE 5 Rotation at 4°C observed with 150-nm or 100-nm gold beads. (*a*) Comparison of time-averaged rotation rates at 2 mM ATP between beads of different sizes. Small triangles are individual rates over >100 consecutive revolutions (except for two triangles for 0.29-μm beads that made 16 and 40 revolutions), and squares their averages ($n \geq 6$), with error bars showing the standard deviations. The 100-nm and 150-nm gold beads averaged 8.9 ± 2.6 and 11.4 ± 2.5 revolutions s^{-1} (rps), respectively, and 0.29-μm plastic beads (also in Fig. 6 *a*) 5.6 ± 2.1 rps. Whether these beads were single or duplex was difficult to ascertain. (*b*) A time course of rotation with a 100-nm gold bead (or duplex) at 2 mM ATP, captured at 2000 frames s^{-1}. The three curves are continuous, with some overlaps at ends. Horizontal solid lines are separated by 120°, and dotted lines are placed 40° below. (*Upper inset*) Histogram of angular positions for the indicated time course, with side peaks at ~80° positions (*arrows*). Not all beads showed clear side peaks. (*Lower inset*) Trajectory of the bead centroid.

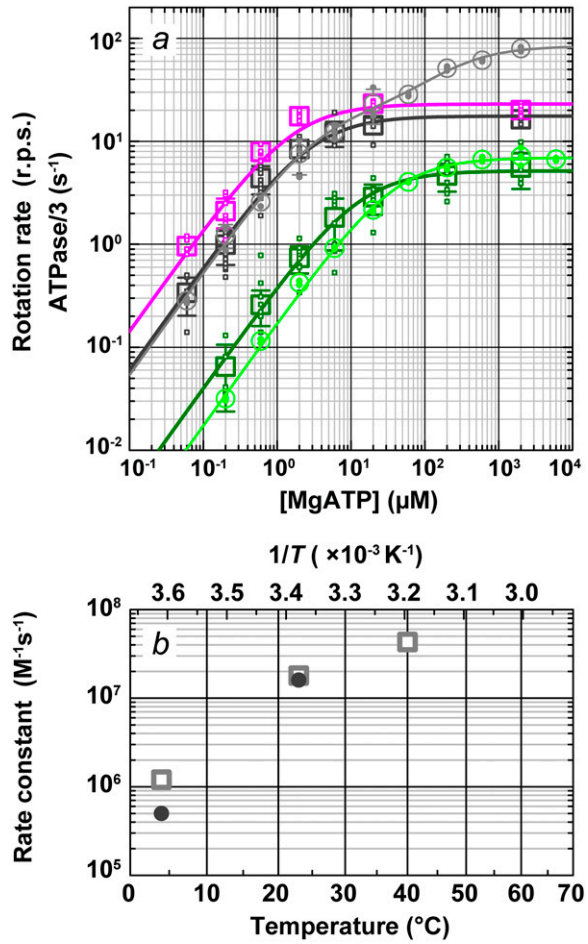

FIGURE 6 Comparison of rotation and hydrolysis rates. (*a*) ATP dependence of the rotation rates (*squares*) and one-third of the initial hydrolysis rates (*circles*). Dark green (rotation) and green (hydrolysis), 4°C; black and gray, 23°C; magenta, rotation at 40°C. Small symbols are individual rates, and large symbols their average ($n \geq 5$ for rotation and $2 \leq n \leq 4$ for hydrolysis); error bars show the standard deviation larger than the symbol size. Individual rotation rates are the time average over >5 consecutive revolutions (usually >100) for a 0.29-μm bead or its duplex. Curves show fit with Michaelis-Menten kinetics: $V = V_{max}[ATP]/(K_m + [ATP])$. For rotation, V_{max} and K_m are 5.2 rps and 13 μM at 4°C (*dark green*), 18 rps and 2.9 μM at 23°C (*black*), and 23 rps and 1.6 μM at 40°C (*magenta*). For hydrolysis, $3 \times V_{max}$ and K_m are 21 s^{-1} and 40 μM at 4°C (*green*). Hydrolysis at 23°C (*gray*) required two sets of parameters: $V = (V_{max1}K_{m2}[ATP] + V_{max2}[ATP]^2)/([ATP]^2 + K_{m2}[ATP] + K_{m1}K_{m2})$, with $3 \times V_{max1} = 59\ s^{-1}$, $K_{m1} = 3.7\ \mu$M, $3 \times V_{max2} = 252\ s^{-1}$, and $K_{m2} = 246\ \mu$M. (*b*) Temperature dependence of the apparent rate of ATP binding estimated from the data in *a* ($3 \times V_{max}/K_m$; *squares*, rotation; *circles*, hydrolysis).

the rotation of 0.29-μm beads are close (Fig. 6 *a*). Moreover, the small gold beads (Fig. 5 *a*) showed rotation rates of ~10 revolutions s^{-1} at 2 mM ATP, which are higher than the hydrolysis rate and in line with the trend seen at lower ATP concentrations. The time-averaged rotary speed of the gold beads is limited by the dwells at or near the ATP-waiting angles (Fig. 5 *b*), not by the drag against rotation which would manifest as a finite slope of stepping time courses (the drag effect was not negligible with 0.29-μm beads as seen in Fig. 4 *g*). The same dwells must also limit the rate of unloaded hydrolysis. That is, a reaction(s) at the ~0° dwell limits the rate of overall catalysis at 4°C, whether a (small) bead is attached or not. This rate-limiting reaction cannot be ATP binding, because k_{on}^{app} at 4°C of $1.2 \times 10^6\ M^{-1}\ s^{-1}$ for rotation or $0.5 \times 10^6\ M^{-1}\ s^{-1}$ for hydrolysis (Fig. 6 *b*) implies a rate of ATP binding of $2.4 \times 10^3\ s^{-1}$ or $1.0 \times 10^3\ s^{-1}$ at 2 mM ATP, far greater than the observed saturating rate of 20–30 s^{-1} ($3 \times V_{max}$ in Fig. 6 *a* or 3 × the rotation rate in Fig. 5 *a*). We have yet to fully identify the nature of this hitherto unresolved rate-limiting reaction at ~0°, which precedes or follows the ATP binding reaction.

Temperature dependence of rotary torque

The saturating levels of time-averaged rotary speed in Fig. 6 *a* are inversely proportional to the viscosity of water

(somewhat lower at 4°C because saturation at this temperature is due mainly to the hitherto unresolved reaction above), suggesting that the torque of the F_1-motor does not change appreciably with temperature. To estimate the torque at various temperatures, we overlay 30 consecutive 120° steps of 0.49-μm beads (mainly a single bead and a duplex in a few cases) at 2 mM ATP and calculate their average (Fig. 7, *thick cyan lines*). At 23°C and above, rotation was basically continuous, with a nearly constant speed, implying a nearly angle-independent torque. The torque values estimated by linear fit to the entire time course (Fig. 7, *a–d*, *straight blue lines*) and using Eq. 2 are plotted in blue in Fig. 7 *f* (*circles* indicate duplex beads). This fitting was unsuccessful at 4°C, where the rotation was clearly stepwise (Fig.7 *e*), and the fit at 10°C was also poor (Fig. 7 *d*). At higher temperatures, too, there was a tendency for the bead to stumble at particular angles, likely ~80° (18), leading to a lower time-averaged speed. The torque values estimated in the central 30–90° portions of the 120° steps (Fig. 7, *a–e*, *straight red lines*) are shown in red in Fig. 7 *f*. For the reasons stated above, we think that the red symbols in Fig. 7 *f* better describe torque. Apparently, the torque produced by the F_1 motor does not

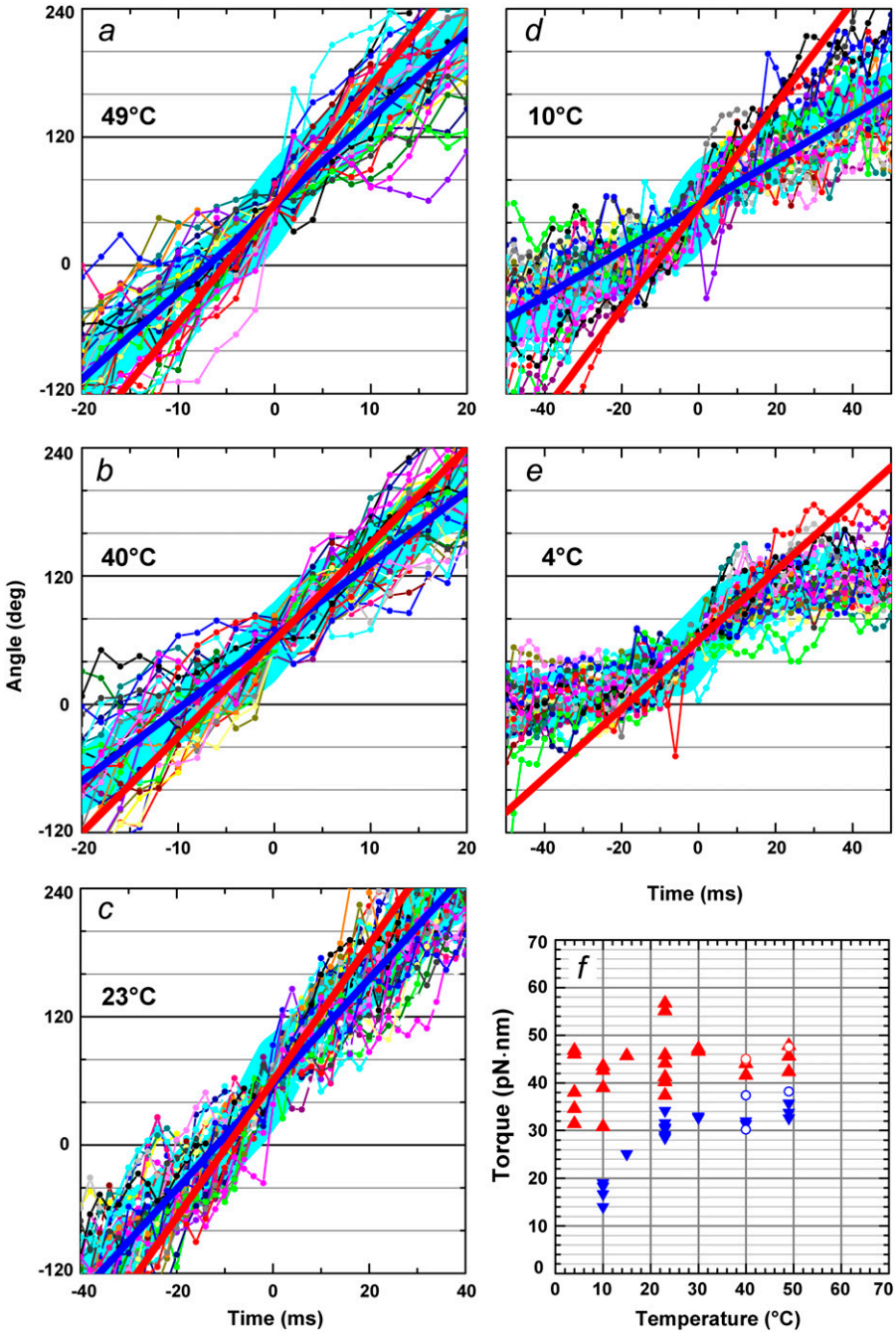

FIGURE 7 Temperature dependence of the torque at 2 mM ATP. (*a–e*) Stepping records for a single 0.49-μm bead. Thin lines with dots show 30 consecutive steps selected from a rotation time course, with their average (*thick cyan line*). Individual step records have been shifted vertically by a multiple of 120° to obtain the overlap. Angle zero was chosen such that most of the pauses (or stumbling) in the time course fall on a multiple of 120°. Time zero for each step record was assigned by eye to the data point closest to 60°. Straight red lines show linear fit to the thick cyan line between 30 and 90°, and straight blue lines to the entire time course encompassing the 30 steps. (*f*) Summary of torque values estimated from Eq. 1 and the slope of the fitted straight line. Red triangles show fits to individual bead records over the 30–90° portion (*a–e*, *red lines*), and blue triangles over the entire time course (*a–d*, *blue lines*). Circles show torque values estimated for 0.49-μm bead duplexes; in this case, the frictional drag coefficient, ξ, in Eq. 1 is given by $\xi = 2 \times 8\pi\eta a^3 + 6\pi\eta a x_1^2 + 6\pi\eta a x_2^2$, where x_1 and x_2 are the radii of rotation (x_1 was taken as zero).

vary appreciably with temperature between 4°C and 50°C. This may be anticipated if the torque is derived from potential (or conformational) energies (5).

DISCUSSION

The rate-limiting process at 4°C

Beef heart mitochondrial F_1 has been shown to dissociate into subunits around 4°C and lose ATP hydrolysis activity (24,25). Our thermophilic F_1 is active over 0–90°C (14,26), and it rotates at 4°C with a torque similar to that at higher temperatures (Fig. 7). Thanks to this higher stability, we have been able to find a hitherto unresolved rate-limiting process at 4°C.

A likely candidate for this process is ADP release. When rotation is forced to slow down by an external force, the ATP that is bound at 0° (an ATP-waiting angle) is released as ADP after 240° of rotation (11). The implication is that, of the three catalytic sites, two are always filled with a nucleotide during slow rotation. During rotation without an external force, spontaneous release of ADP at 240° (another ATP-waiting angle) is slow, of the order of 1 s^{-1} or likely much slower (11). Binding of the next ATP at 240°, filling the third catalytic site, initiates further rotation beyond 240°, which promotes the release of ADP. This rotation beyond 240° must increase the rate of ADP release sharply in an angle-dependent fashion: with thermophilic F_1 at room temperature, the effective release rate must reach $>10^4$ s^{-1} by 360°, because the ATP-waiting dwell at 360° is very short and at most 10^{-4} s (11,12), implying that the binding site is already vacated by 360°. Based on this scheme for the timing of ADP release at 23°C, there are at least two possible scenarios for the ADP release to be rate-limiting at 4°C: 1), ADP fails to dissociate by 360°, preventing the next ATP, to be bound at 360°, from entering the binding site; or 2), the ATP-induced ADP release at 240° is slow at 4°C, preventing rotation from ~240° toward 360°. Either scenario implies that the activation energy for ADP release is higher than those for other processes.

The scheme above for the timing of ADP release at 23°C is based on the behavior of a fluorescent ATP analog (11), and may not apply to reactions involving unlabeled ATP. There have been reports that suggest that ADP release occurs before ATP binding and thus F_1 operates in the so-called bisite scheme where the nucleotide occupancy of the three catalytic sites alternates between one and two (27,28) as opposed to two and three (mostly two) in our scheme (11) or in an earlier proposal (29). This site-occupancy issue is yet unsettled, and possibilities other than the rate-limiting process being ADP release cannot be ruled out. For example, a conformational change that takes place near ATP-waiting angles, either before or after ATP binding, could be rate-limiting at 4°C. Addition of ADP in the medium should in principle give a hint as to whether ADP release is indeed rate-limiting, but MgADP inhibition hampers such experiments.

Temperature dependence of various rate constants

For a homogenous population of an enzyme, reaction rates can be assessed in a bulk solution, which allows precise measurements. F_1-ATPase, however, is almost always inhomogeneous, one part being active and the other inhibited. Immediately after the addition of nucleotide-free F_1, one could expect most, if not all, F_1 molecules to be active, but in this study, we have found that this is not so at high temperatures when temporal resolution is limited. Above 35°C, F_1 becomes an equilibrium mixture of active and inhibited populations within 2 s, with the inactive population dominant. Apparent time independence of the activity, as seen at 35–50°C, does not necessarily imply that all population is active, a conclusion we might have drawn had we not explored an extensive temperature range. That F_1 rapidly falls in the inhibited state at high temperatures is reasonable, because its physiological role is ATP synthesis, not consumption of ATP, and the physiological temperature of the thermophilic F_1 is near 70°C.

All rates that we have measured in this study increase with temperature, which is expected for a protein machine until it starts to denature at a high temperatures. In the previous study (14), the hydrolysis activity, measured as the amount of phosphate released over a period of 10 min, showed a distinct peak at 20°C, whereas the steady-state activity in Fig. 3 *a* continues to increase with temperature. This apparent discrepancy is explained by the fact that, at ~20°C, the initial rapid hydrolysis persists for tens of seconds (Fig. 2), during which a considerable amount of phosphate accumulates. The initial burst is negligible above 30°C.

Except for the hydrolysis and rotation activities below ~10°C, the increase in rate constants over a 10°C interval (Q_{10}) was severalfold (Figs. 3 *a* and 6 *b*), which is common in many biochemical reactions. The steep temperature dependence of the activities below ~10°C is indicative, but by no means proof, of the appearance of a different rate-limiting process. By observing rotation of individual molecules, we have been able to show that, whereas ATP hydrolysis and phosphate release that take place at 80° positions limit the overall rate of catalysis at room temperature, a different reaction(s) at ~0° positions is rate-limiting at 4°C. The latter is likely ADP release, but we have yet to fully confirm this interpretation.

We thank M. Shio for designing a stable microscope stage, R. Kanda for sample preparation, Y. Onoue and A. Palanisami for critical discussion, K. Sakamaki and M. Fukatsu for encouragement and lab management, and members of the Kinosita lab for help and advice.

This work was supported by Grants-in-Aid for Specially Promoted Research and for Young Scientists (B) and the 21st Century COE Program

from the Ministry of Education, Sports, Culture, Science and Technology-Japan.

REFERENCES

1. Abrahams, J. P., A. G. W. Leslie, R. Lutter, and J. E. Walker. 1994. Structure at 2.8 Å resolution of F_1-ATPase from bovine heart mitochondria. *Nature*. 370:621–628.
2. Boyer, P. D. 1997. The ATP synthase—a splendid molecular machine. *Annu. Rev. Biochem.* 66:717–749.
3. Noji, H., R. Yasuda, M. Yoshida, and K. Kinosita Jr. 1997. Direct observation of the rotation of F_1-ATPase. *Nature*. 386:299–302.
4. Yoshida, M., E. Muneyuki, and T. Hisabori. 2001. ATP synthase—a marvellous rotary engine of the cell. *Nat. Rev. Mol. Cell Biol.* 2:669–677.
5. Kinosita, K., Jr., K. Adachi, and H. Itoh. 2004. Rotation of F_1-ATPase: how an ATP-driven molecular machine may work. *Annu. Rev. Biophys. Biomol. Struct.* 33:245–268.
6. Yasuda, R., H. Noji, K. Kinosita Jr., and M. Yoshida. 1998. F_1-ATPase is a highly efficient molecular motor that rotates with discrete 120° steps. *Cell*. 93:1117–1124.
7. Adachi, K., R. Yasuda, H. Noji, H. Itoh, Y. Harada, M. Yoshida, and K. Kinosita Jr. 2000. Stepping rotation of F_1-ATPase visualized through angle-resolved single-fluorophore imaging. *Proc. Natl. Acad. Sci. USA*. 97:7243–7247.
8. Nishizaka, T., K. Oiwa, H. Noji, S. Kimura, E. Muneyuki, M. Yoshida, and K. Kinosita Jr. 2004. Chemomechanical coupling in F_1-ATPase revealed by simultaneous observation of nucleotide kinetics and rotation. *Nat. Struct. Mol. Biol.* 11:142–148.
9. Itoh, H., A. Takahashi, K. Adachi, H. Noji, R. Yasuda, M. Yoshida, and K. Kinosita Jr. 2004. Mechanically driven ATP synthesis by F_1-ATPase. *Nature*. 427:465–468.
10. Rondelez, Y., G. Tresset, T. Nakashima, Y. Kato-Yamada, H. Fujita, S. Takeuchi, and H. Noji. 2005. Highly coupled ATP synthesis by F_1-ATPase single molecules. *Nature*. 433:773–777.
11. Adachi, K., K. Oiwa, T. Nishizaka, S. Furuike, H. Noji, H. Itoh, M. Yoshida, and K. Kinosita Jr. 2007. Coupling of rotation and catalysis in F_1-ATPase revealed by single-molecule imaging and manipulation. *Cell*. 130:309–321.
12. Yasuda, R., H. Noji, M. Yoshida, K. Kinosita Jr., and H. Itoh. 2001. Resolution of distinct rotational substeps by submillisecond kinetic analysis of F_1-ATPase. *Nature*. 410:898–904.
13. Shimabukuro, K., R. Yasuda, E. Muneyuki, K. Y. Hara, K. Kinosita Jr., and M. Yoshida. 2003. Catalysis and rotation of F_1 motor: cleavage of ATP at the catalytic site occurs in 1 ms before 40° substep rotation. *Proc. Natl. Acad. Sci. USA*. 100:14731–14736.
14. Yoshida, M., N. Sone, H. Hirata, and Y. Kagawa. 1975. A high stable adenosine triphosphatase from thermophilic bacterium. Purification, properties, and reconstitution. *J. Biol. Chem.* 250:7910–7916.
15. Adachi, K., H. Noji, and K. Kinosita Jr. 2003. Single-molecule imaging of rotation of F_1-ATPase. *Methods Enzymol.* 361B:211–227.
16. Matsui, T., E. Muneyuki, M. Honda, W. S. Allison, C. Dou, and M. Yoshida. 1997. Catalytic activity of the $\alpha_3\beta_3\gamma$ complex of F_1-ATPase without noncatalytic nucleotide binding site. *J. Biol. Chem.* 272:8215–8221.
17. Noji, H., D. Bald, R. Yasuda, H. Itoh, M. Yoshida, and K. Kinosita Jr. 2001. Purine but not pyrimidine nucleotides support rotation of F_1-ATPase. *J. Biol. Chem.* 276:25480–25486.
18. Sakaki, N., R. Shimo-Kon, K. Adachi, H. Itoh, S. Furuike, E. Muneyuki, M. Yoshida, and K. Kinosita Jr. 2005. One rotary mechanism for F_1-ATPase over ATP concentrations from millimolar down to nanomolar. *Biophys. J.* 88:2047–2056.
19. Weast, R. C. 1988. CRC Handbook of Chemistry and Physics, 69th ed. CRC Press, Boca Raton, FL.
20. Svoboda, K., and S. M. Block. 1994. Biological applications of optical forces. *Annu. Rev. Biophys. Biomol. Struct.* 23:247–285.
21. Jault, J. M., C. Dou, N. B. Grodsky, T. Matsui, M. Yoshida, and W. S. Allison. 1996. The $\alpha_3\beta_3\gamma$ subcomplex of the F_1-ATPase from the thermophilic *Bacillus* PS3 with the β T165S substitution does not entrap inhibitory MgADP in a catalytic site during turnover. *J. Biol. Chem.* 271:28818–28824.
22. Hirono-Hara, Y., H. Noji, M. Nishiura, E. Muneyuki, K. Y. Hara, R. Yasuda, K. Kinosita Jr., and M. Yoshida. 2001. Pause and rotation of F_1-ATPase during catalysis. *Proc. Natl. Acad. Sci. USA*. 98:13649–13654.
23. Bertazzon, A., and T. Y. Tsong. 1990. Effects of ions and pH on the thermal stability of thin and thick filaments of skeletal muscle: high-sensitivity differential scanning calorimetric study. *Biochemistry*. 29: 6447–6452.
24. Chernyak, B. V., V. Ya. Chernyak, T. B. Gladysheva, Z. E. Kozhanova, and I. A. Kozlov. 1981. Structural rearrangements in soluble mitochondrial ATPase. *Biochim. Biophys. Acta*. 635:552–570.
25. Penefsky, H. S., and R. C. Warner. 1965. Partial resolution of the enzymes catalyzing oxidative phosphorylation. VI. Studies on the mechanism of cold inactivation of mitochondrial adenosine triphosphatase. *J. Biol. Chem.* 240:4694–4702.
26. Yoshida, M., N. Sone, H. Hirata, and Y. Kagawa. 1977. Reconstitution of adenosine triphosphatase of thermophilic bacterium from purified individual subunits. *J. Biol. Chem.* 252:3480–3485.
27. Milgrom, Y. M., and R. L. Cross. 2005. Rapid hydrolysis of ATP by mitochondrial F_1-ATPase correlates with the filling of the second of three catalytic sites. *Proc. Natl. Acad. Sci. USA*. 102:13831–13836.
28. Bulygin, V. V., and Y. M. Milgrom. 2007. Studies of nucleotide binding to the catalytic sites of *Escherichia coli* βY331W-F_1-ATPase using fluorescence quenching. *Proc. Natl. Acad. Sci. USA*. 104:4327–4331.
29. Weber, J., and A. E. Senior. 2001. Bi-site catalysis in F_1-ATPase: does it exist? *J. Biol. Chem.* 276:35422–35428.